Dynamic response of low-aspect-ratio cantilever NACA0012 airfoil at low-to-moderate Reynolds numbers

S. Martínez-Aranda[a], A. L. García-González[b,*], L. Parras[b], J.F. Velázquez-Navarro[b], C. del Pino[b]

[a] *Faculdade de Engenharia da Universidade do Porto, Departamento de Engenharia Mecânica, Rua Dr. Roberto Frias s/n, 4200-465 Porto, PORTUGAL*
[b] *Universidad de Málaga, E.T.S. Ingeniería Industrial, Campus de Teatinos s/n, 29071 Málaga, SPAIN*

Abstract

The influence of the angle of attack (AoA) and the chord based Reynolds number (Re_c) on the lift and drag coefficients has been analyzed experimentally in a low-aspect-ratio NACA0012 airfoil, AR=2. The tests have been carried out in a low turbulence wind tunnel with a digital force sensor. Results are shown for chord based Reynolds numbers in the range $3.33 \cdot 10^4 \leq Re_c \leq 1.33 \cdot 10^5$ and AoA between -0° and +35°. The dynamic response of the wing has been studied using time-frequency analysis. We compute the Power Spectral Density (PSD) from the temporal evolution of the net force exerted over the wing, showing that the main response of the wing is the presence of two natural frequencies of the wing-base system. Again, the mean PSD suddenly increases for $Re_c \approx 1 \cdot 10^5$, particularly at AoA exceeding the (stall) critical point. Finally, and despite from the fact that our model is rigid, we find PSD peaks at very low and high frequencies in agreement with other authors' results which correspond to energetic modes in the wing-tip vortex and the formation and emission of coherent (unstable) turbulent structures, respectively.

Keywords:
Finite wing, Low Re aerodynamics, Wing-tip vortex, Dynamic response, Fundamental vibration frequencies.

1. Introduction

A wing profile is a surface that may be designed to provide the maximum lift force with the minimum drag. The relationship between both forces is determined by the wing cross section aerodynamics features (1). In finite wings at low Reynolds numbers, the drag and the lift coefficient variations are mainly due to three mechanisms: Wing-tip vortex (2; 3; 4; 5); laminar boundary layer separation leading to the formation of a laminar separation bubble (LSB) and the subsequent turbulent separated shear layer (6; 7; 8); and, finally, the vortex shedding in the wake behind the wing (9; 10; 11). Most of these numerical or experimental investigations were performed analyzing only the flow behaviour. Hence, the C_D and C_L experimental measurements involve a whole fluid-structure scenario, giving us an overview of the interaction between the wing and the flow that passes over it. For this reason, a dynamic response analysis of a cantilever with low-aspect-ratio NACA0012 profile is considered in this paper together with the C_D and C_L classical measurements in a wind-tunnel. The aim of this novel analysis is to study the possible relationships among wing-tip vortex, surface flow regimes, wake vortex and structural dynamic response.

The study of the dynamic response of rigid wing models, the flow behaviour in the suction surface and the wake have been extensively studied for a wide range of airfoils at low Reynolds numbers. (12) characterized the flow regimes in the suction surface of a NACA 0012 airfoil for $3 \cdot 10^4 < Re_c < 1.3 \cdot 10^5$ and

*Corresponding author: tolin@uma.es

$AR = 5$. (9) reported that the evolution of vortex shedding behind the airfoil at small AoA is connected to the behaviour of shear-layer instabilities. Coherent turbulent structures generated in the separated shear-layer region, interact in the turbulent wake creating a large-scale vortex with mesured frequencies one order of magnitude lower than the fundamental frequency of the shear-layer disturbances. The vortex shedding frequency behind a NACA 0012 airfoil was also measured by (10). Four emission modes were identified: laminar, subcritical, transitional and supercritical. Similar results for others symmetric airfoils can be found in literature, e.g. NACA0018 and NACA0025 (13; 14; 15).

There are experimental data for 2D NACA 0012 airfoils mounted on two supports and covering low Reynolds numbers between $5.3 \cdot 10^3$ and $5.1 \cdot 10^4$ (16; 17). It has been also studied the pitching oscillation of NACA0012 airfoils (18; 19; 20), but these self-sustained oscillation analyses differ from the dynamic response presented in this paper. Actually, the boundary conditions are completely different, because these airfoils have both edges attached, so that wing-tip vortex formation is neglected. There are recent studies concerning eperimental modal analysis for low-aspect-ratio rectangular membrane wings (21; 22). These modal analyses were performed by means of Digital Image Correlation (DIC) technique so, in this case, deformation data were reported and no forces were measured. The ratio between wing deformations and the flow characteristics is also reported in the State of Art. Rojratsirikul (21; 22) suggested a possible coupling between the membrane vibration with the onset of wake instabilities for all airfoils. To shed some new light into this problem, we have analyzed in this work the dynamic response, despite of the stiffness differences between elastic membranes and the rigid aluminum NACA0012 airfoil used in this experimental work.

Other key aspect which has been studied in detail consists of the noise production as several types of NACA airfoils are immersed in turbulent flow streams (23; 24; 25; 26). Moreau analyzed the noise produced by finite airfoil at low-to-moderate Reynolds numbers. Appart from the noise measurements, surface oil-film visualization images were also taken in order to determine flow mechanisms responsible of noise generation. In this manner, our research study is a complement to attain only an objective view of airfoil vibration. On the other hand, Chong (24) studied the noise differences between straight and serrated trailing edges by means of Particle Imaging Velocimetry (PIV) measurements of the NACA0012 airfoil wakes together with microphones. Besides, these authors found that small variations in AoA can lead to noise level increments due to laminar separation bubble. Devenport (26) carried out leading edge noise measurements on three different NACA airfoils immersed in turbulent regime. Also, a noise increment with AoA was observed. As will be commented below, similar conclusions can be deducted from our experimental study. Our motivation is based on the belief that experimental information of wing profile vibrations would be relevant for problems of fluid-structure interaction (FSI), and numerical model validations which have been also used for airfoil noise estimation, e.g. (27; 28).

2. Experimental arrangement

Experimental tests set can be followed in previous papers (see 29; 30). An schematic drawing is shown in Figure 1 (see Fig. 1). The turbulence level (Turbulence Intensity I [%]) is shown in Table 1.

The standard deviation of the tests will be presented and discussed in Section 3.

3. Aerodynamic characteristics: results and discussion

3.1. Coefficient deviations and errors

Fig. 2 (a) shows the data together with errorbars that corresponds to standard deviations from the average values of the drag and lift coefficients as function of AoA for $\alpha = 0°$ - $35°$ at Reynolds numbers $Re_c = 1.33 \cdot 10^5$, which represents the worst case dealing with measurement errors. Other cases analyzed in this work show a similar behaviour. Actually, the deviation remains constant up to the stall angle ($\alpha \leq 12°$ - $14°$) and these variations are close to $\pm$ 0.025 in both coefficients, C_L and C_D. As it can be also observed in Figs. 2 (b) and (c), that absolute values of the standard deviations with AoA smaller

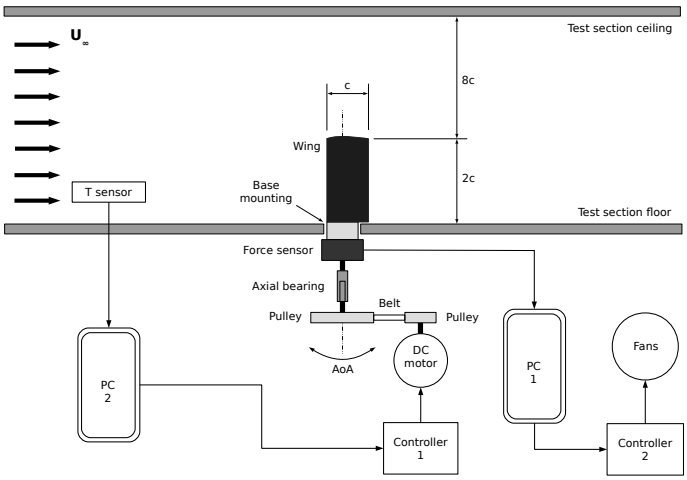

Figure 1: Schematic of the experimental setup.

$\%P$	U_∞ $[m/s]$	$\delta U_\infty [m/s]$	Re_c	$I[\%]$
0.68	5	$\pm$ 0.06	$3.33 \cdot 10^4$	1.2
11.25	10	$\pm$ 0.12	$6.67 \cdot 10^4$	1.2
21.43	15	$\pm$ 0.16	$1 \cdot 10^5$	1.1
30.56	20	$\pm$ 0.47	$1.33 \cdot 10^5$	2.3

Table 1: Percentage of power, wind velocities and their variations, chord based Reynolds numbers and levels of turbulence intensity.

than 12° remain constant for any value of the Reynolds numbers. At AoA equal to or slightly greater than stall, a great fluctuation appears in the force signal, resulting in a sudden increment of the C_L and C_D deviations. We observe self-sustained oscillations in the cantilever at these AoA. The maximum values of coefficient deviations take place for AoA between 12° and 20° in all cases and they are always lower than 15%, approximately. These deviations in the coefficients gradually decrease at AoA greater than 20° for any value of Re_c. Experimentally, one can observe in this range of AoA shrinking wing vibrations. Consequently, the variations in the force amplitude diminish. However, for the lowest chord based Reynolds number $Re_c = 3.33 \cdot 10^4$ the coefficient deviations almost remain constant regardless the AoA.

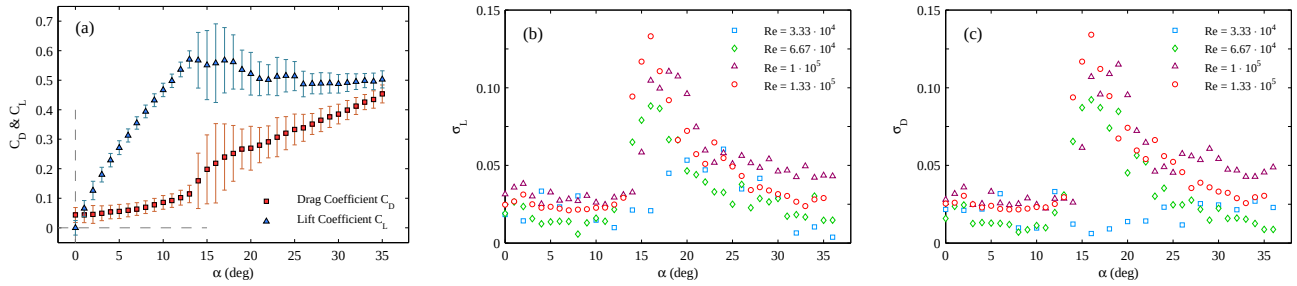

Figure 2: Mean and standard deviation of C_D and C_L for $Re_c = 1.33 \cdot 10^5$ (a); standard deviations in the lift, σ_L (b) and drag, σ_D coefficients (c) for all AoA and Reynolds numbers.

Kline (31) developed the method to compute the propagation of experimental measurement errors, so one can estimate the accuracy of the non-dimensional drag and lift coefficients. Considering their formulation to determine the aerodynamic coefficients, large percentage uncertainties appear for coefficients approaching zero. The accuracy of the force measurement is 0.01 N, the rotational device has a resolution of 0.1°, and the accuracy of the free-stream velocity using LDA is within 1% (32). Table 2 shows the estimation of the average errors for C_D and C_L at each Reynolds number, thus confirming a good experimental procedure in the computation of these coefficients because the fluctuation measurements are done with acceptable precision. Only C_D and C_L average values will be presented in the following section.

Re_c	% *Error* C_D	% *Error* C_L
$3.33 \cdot 10^4$	$\pm$ 8.6	$\pm$ 6.2
$6.67 \cdot 10^4$	$\pm$ 3.1	$\pm$ 2.0
$1 \cdot 10^5$	$\pm$ 1.7	$\pm$ 1.3
$1.33 \cdot 10^5$	$\pm$ 1.4	$\pm$ 1.2

Table 2: Average errors for coefficients C_D and C_L.

3.2. Drag and Lift Curves

Drag coefficients are depicted in Fig. 3 as function of α. Our results show a slight deviation in comparison to those obtained by Ngo (33). Besides, our values of C_{Dmin} are in agreement with those reported by Mueller (3) for a flat wing with the same aspect ratio and Reynolds numbers. Regarding the ratio between drag coefficient and AoA, $\Delta C_D/\Delta\alpha$, we observe an increment of its value up to the stall angle, so that the wing loses its aerodynamic effectiveness. Different slopes are found at each Reynolds number, increasing the values of the slope with the AoA up to the stall angle.

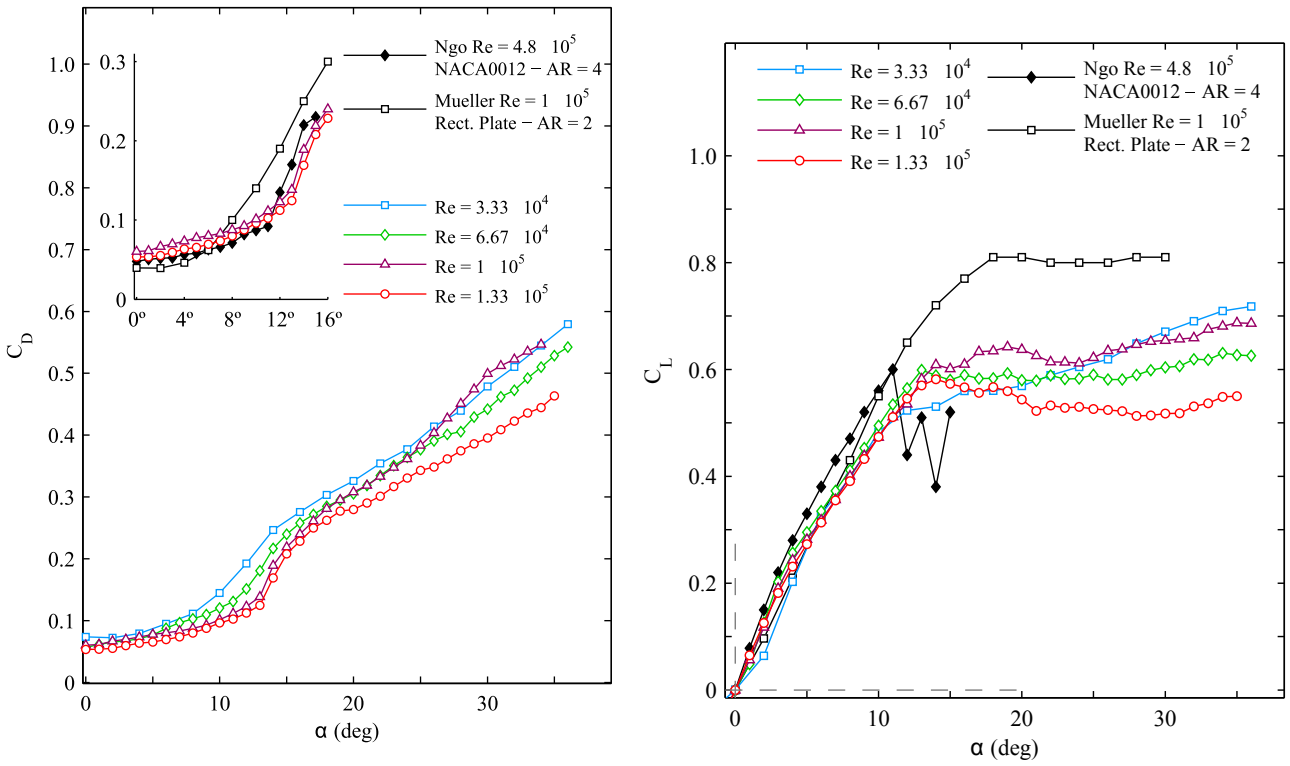

Figure 3: C_D and C_L curves as function of α for all Reynolds numbers tested (a) C_D vs α for any value of the Reynolds numbers, as indicated. The inset represents a detail of C_D values for low AoA and high Reynolds numbers together with those reported by (33) and (3). (b) C_L vs α for any value of the Reynolds numbers together with those reported by (33) and (3).

The maximum lift coefficient C_{Lmax} ranges between 0.52 and 0.61 for any value of the Reynolds numbers, and the stall angles α_{stall} appear between 12 and 14 degrees. These values show a slight deviation compared to those published by (33) with AR=4. As expected, our stall angles are slightly greater than Ngo's results due to the aspect ratio reduction (AR=2 in our case). It is worth mentioning that the values of C_L are lower than those obtained by Mueller (3) for a flat plate with the same aspect ratio and Reynolds numbers.

4. Wing dynamic response: results and discussion

The temporal evolution of the force acting on the wing has been analyzed for any value of the AoA and four values of the Reynolds numbers. We calculate the power spectral density (PSD) for each signal in the frequency domain by means of a FFT built-in *Matlab*® function. We subtract the mean force to the instantaneous one, thus obtaining the temporal evolution of the force and the most energetic frequencies. As it was stated above, the sampling frequency of the force sensor is $f_s = 250$ Hz, and the time recording of the tests is $T = 200$ s, hence the frequency resolution is $df = \pm 0.005$ Hz. We consider a low-pass filter in order to avoid aliasing effects in the digital signal. After applying this filter, the frequencies beyond the Nyquist ones are removed, being $F_{Nyquist} = f_s/2$.

We obtain the natural frequencies of the wing-base system with two sets of ten tests with no velocity inside the wind tunnel. The first testing consists of an instant impact at the free ending in the wing center following a direction perpendicular to the chord. Thus, the model vibrates freely and we record the net

force. The temporal signal is analyzed by means of the FFT function. A main free vibration frequency is detected at $f_{1st} \approx 28.25$ Hz. The second testing consists of an instant impact at the cylindrical aluminum base which fixes the wing to the force sensor. We detect the main frequency f_{1st} in all the tests. However, a second frequency appears at $f_{2nd} \approx 43.50$ Hz. Therefore, f_{1st} and f_{2nd} are the first and the second natural frequencies of the wing-base system depicted in Fig 1.

As a simple theoretical model, one can estimate the natural frequency using as a model of the aluminium NACA0012 airfoil a flat plate with the same inertial thickness. The natural vibration frequencies for a rectangular aluminum plate were already obtained experimentally by Dalley (34). The rectangular plate had an aspect ratio $AR = 2$, perfectly embedded in one of its short edges and free at the other. Dalley observed an eigenvalue of the vibration problem for the first natural mode $\lambda = \omega \cdot a^2 \cdot \sqrt{\rho/D} = 3.36$, where ω is the first mode frequency, a the length of the plate, ρ material density and $D = E \cdot h^3/[12 \cdot (1 - \mu^2)]$ the bending modulus of the plate (E is the material Young modulus, h the plate thickness and μ the Poisson module). We consider an equivalent rectangular solid plate with the same moment of inertia I, the same cross-sectional area a_t and the same aspect ratio AR of our model, the NACA0012 airfoil. The frequency computed is similar to a free vibration frequency in the first mode of 29.43 Hz, very close to that obtained experimentally for our model. In addition, the frequencies of the first three natural vibration modes of the equivalent plate have been also calculated analytically by means of the formulation developed by Warbuton (35). For the equivalent rectangular solid aluminum plate described above, the frequency for the first symmetric deformation mode is 30.81 Hz. This first mode has the smallest characteristic frequency and it requires less energy input to be produced than other modes. The frequencies obtained for the second and the third natural vibration modes are 154.56 Hz and 192.97 Hz, respectively. The theoretical values of frequency for the first deformation mode of the equivalent plate are again in agreement with experimental data obtained for the first natural frequency of the wing-base system, f_{1st}. The small differences between theoretical and experimental data may be primarily due to the difference among real and theoretical boundary conditions; and secondly, the difference between NACA0012 profile and its equivalent rectangular plate.

Fig. 4 sums up all the experimental results. It shows the ratio between the PSD and the mean PSD for any value of Re_c and AoA. PSD stems from the temporal evolution of the net force measurements. We only depict normalized PSD with power greater than five times the mean PSD. Moreover, we plot frequencies for vortex shedding in the near field of the wake reported by Huang (9) and Lee (10) in squares and diamonds, respectively. These data have been adapted from their Strouhal number data ($St = f \cdot d/U_\infty$), where d is the length of the wing-section projection on the cross-stream direction. These authors observed that frequencies diminished as the AoA increased. However, the vibration of our model has a strong influence due to mechanical characteristics of the cantilever wing. The net aerodynamic force signal has two important sinusoidal components that correspond to natural frequencies of the wing-base in all cases ($f_{1st} \approx 28.25$ Hz and $f_{2st} \approx 43.50$ Hz). The presence of the most energetic peak at the first natural frequency is independent of the fluid flow around the model, while the peak at the second natural frequency is less dominant and its relative importance depends on Re_c and the AoA. Furthermore, our results could be compared with other work in which the dynamic response of a wing on-two-supports is dominated by the shedding vortex frequency (16). They reported power peaks in the measured force signal at low frequencies ($f \approx$5-10 Hz) regarding large-scale vortex formation (perpendicular to wing-tip vortex) and emission in the wake at large AoA ($\alpha \geq 30^\circ$ and Re_c=$1.05 \cdot 10^4$). Unfortunately, our model offers PSD with peaks at natural frequencies f_{1st} and f_{2nd}. A possible explanation of this discrepancy could be the effect of the different type of airfoil support-setup base system of their experimental arrangement. Their research focused only on the dynamics of a wing on-two-supports, while our experimental study is based on mechanical vibrations produced by fluid structure interaction in a cantilever wing. Given the rigidity of our model, it is evident the strong influence of the mechanical behaviour. Nevertheless, we could find very low and high frequencies which will be analyzed in detail below. We first focus on the effects caused by Reynolds number and AoA.

We depict in Fig. 5 the power spectral density (PSD) as function of frequency for two Reynolds

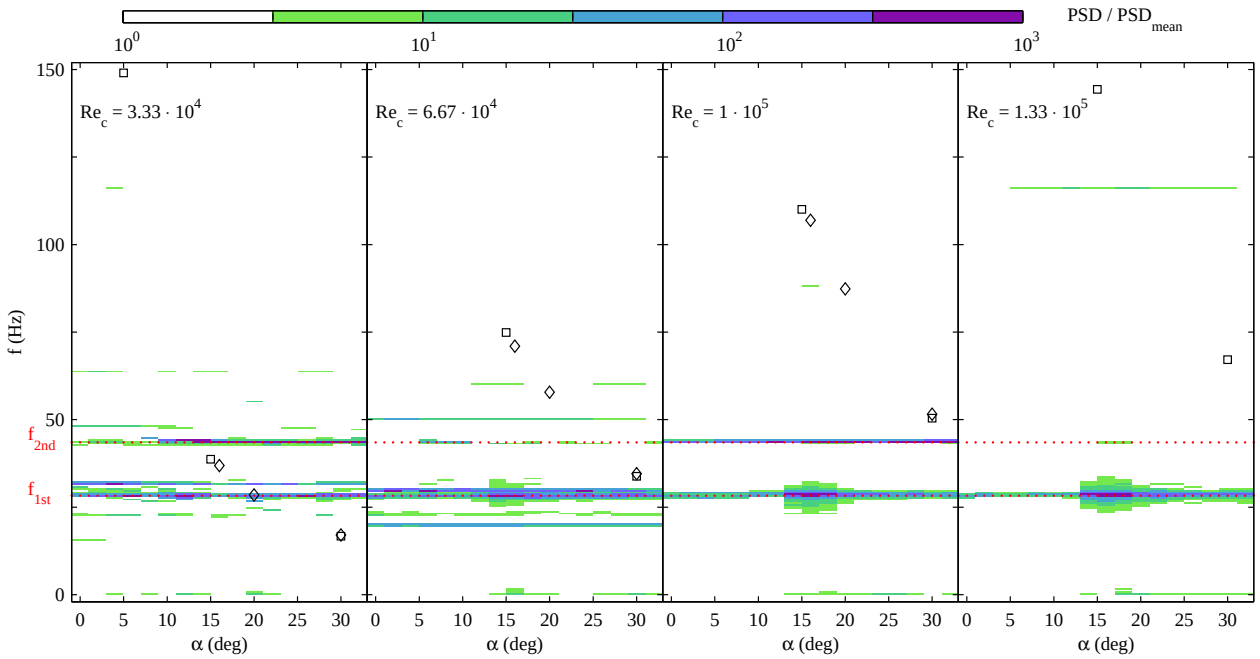

Figure 4: Frequencies given by the normalized PSD ($\mathrm{PSD/PSD_{mean}}$) for four values of Re_c and several AoA from 0° to 35° together with the vortex shedding frequencies in the wake adapted from (9) and (10), plotted in squares and diamonds, respectively.

numbers: $Re_c = 3.33 \cdot 10^4$ (a) and $Re_c = 1.33 \cdot 10^5$ (b), and for several AoA between 0° and 30°. For the lowest Re_c case, the power level of the signal does not depend on the AoA and remains almost constant. For the highest Reynolds number, one can observe again that the PSD remains almost constant at AoA lower than $\alpha = 14°$. Once the (stall) critical point is achieved, the power spectrum is one order of magnitude greater than those presented at low AoA, being more significant at low frequencies. For AoA beyond 20°, the power decreases again, although it continues being more energetic than those given for pre-stall angles.

The increment in the PSD shown in Fig. 5 caused by the vibration process at stall angles is a consequence of the change in the overall flow characteristics, specially on the flow regime in the suction surface of the NACA 0012 airfoil, and the subsequent emission of shear layer instabilities. Laminar separation regime (without subsequent reattachment) dominate the flow at AoA lower than 3°-5° for any value of Re_c considered in this work (see also 12). As the AoA increases beyond a certain threshold, the separated boundary layer reattaches to the surface, thus forming the characteristic laminar separation bubble (LSB) on the surface. At these flow regimes, the fundamental frequency of shear-layer disturbances depends strongly on the Re_c and weakly on the AoA, but it does not show sudden variations (9; 13; 36). However, the separation bubble burst and the resulting transition from LSB regime to a turbulent separated boundary layer, which occurs at the stall angle, causes a sharp drop on the fundamental frequency of the shear layer instabilities (15; 14). This sudden perturbation on the flow characteristics excite the first natural frequency f_{1st} of the cantilever wing (see Fig. 4) since this frequency need the lowest amount of energy to gain power, leading to an increment in the wing vibration amplitude. Thus, the PSD level increases for the whole force signal at the turbulent separation regime (AoA slightly greater than the stall point). The absence of power increment for the lowest Reynolds number together with the lack of a marked lift drop at the stall angle, suggests that turbulent reattachment near the separated shear layer does not fully occur at the NACA 0012 suction surface since this case is slightly lower than the critical Reynolds number for the LSB formation (37; 9). To provide a better understanding of these points, Fig. 6 (a) shows the mean PSD of the net force for the first mechanical frequency $f_{1st} = 28.25 \pm$

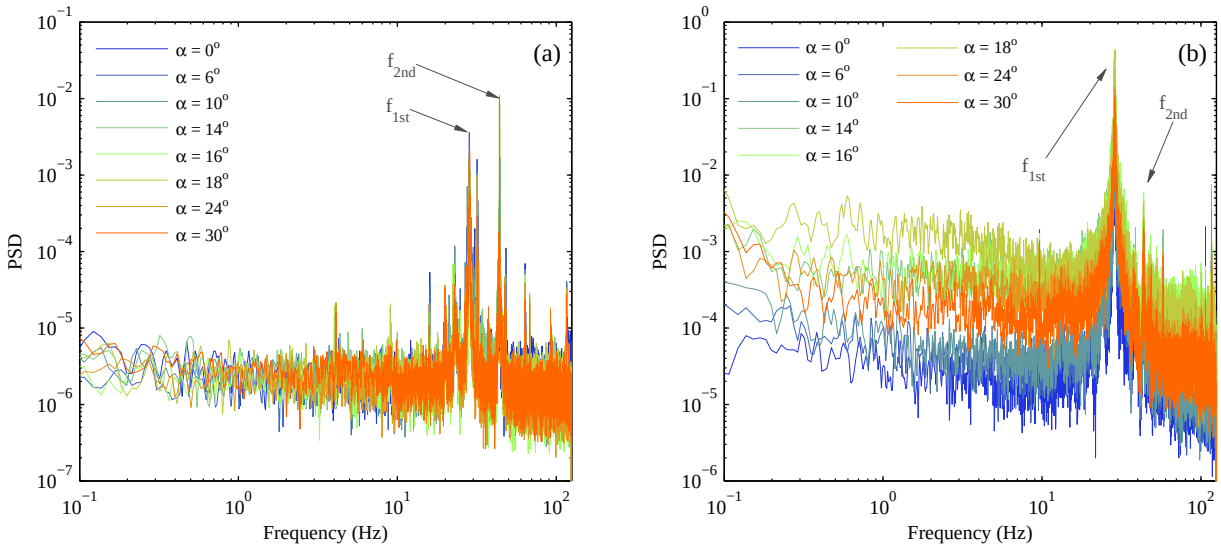

Figure 5: PSD for $Re_c = 3.33 \cdot 10^4$ (a) and $Re_c = 1.33 \cdot 10^5$ (b) for AoA between 0° and 30°.

1.00 Hz, whilst Fig. 6 (b) depicts the mean PSD for the lowest frequencies interval $f_{low} = [0.005, 2.000]$ Hz. There is a increment of power as Re_c increases, but this may be explained due to an increase of the turbulent kinetic energy transported by increasing the value of the free-stream velocity. However, the PSD for the first natural frequency presents a sudden increment when approaching stall, followed by a slow decrease with the AoA, specially for Re_c greater than $1 \cdot 10^5$. This change in the power produces the first natural vibration mode of the cantilever wing to become significant in the dynamic response at stall angles as shown in Fig. 4. Consequently, force fluctuations increment their values as also shown in Fig. 2. The reader must notice that this critical Reynolds number Re_c=$1 \cdot 10^5$ is also connected to the aerodynamic characteristics (30), at which β_{L1} saturates its value and the polar curve changed its trend. Finally, and comparing Figs. 6 (a) and (b), it is worth mentioning that the maximum PSD is reached at frequencies between 0.005 and 2.000 Hz in a smoother form than with the first natural frequency, f_{1st}. This feature stems from the fact that the presence of the stall angle not only strongly affects the power increment at these low frequencies, but also other flow phenomena could be relevant. This analysis will be carried out in the following section.

4.1. Dynamic response at very low frequencies

In order to characterize with detail the power presented at very low frequencies, a new signal is developed by a low-pass 2 Hz filter. Thus, the components of longer time periods are isolated for each AoA and Reynolds number. To improve the experimental observations given in Fig. 4, Fig. 7 shows the PSD of the filtered net force signal ($f \leq 2$ Hz) normalized by the mean power in a logarithmic scale. Peaks appear for frequencies lower than 0.2 Hz, and for any value of the Reynolds number, particularly at large AoA. This low frequency corresponds to the typical development of the wing-tip vortex as the AoA increases for $Re_c = O(10^5)$ (see 5). The value of the most energetic frequency is also in agreement with the experimental results reported in a previous paper(38). In their work, there was a vortex centroid position variation (called vortex meandering) at the plane perpendicular to the flow direction, its frequency being lower than 0.2 Hz for axial positions, x/c, ranging from 0 to 4 (near field) and $22504 \leq Re_c \leq 41874$. For the same phenomenon and using PIV measurements, Roy (39) also reported values for the fundamental frequency of the vortex center variation slightly lower than 1 Hz in a plane located at $x/c = 11.2$ (far

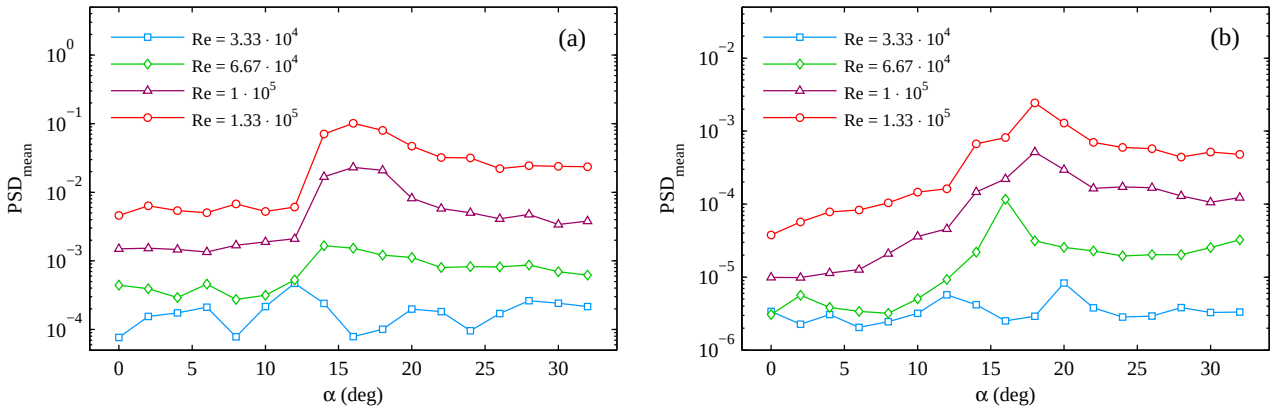

Figure 6: Mean PSD for the first mechanical frequency $f_{1st} = 28.25 \pm 1.00$ Hz (a) and for the lowest frequencies interval $f_{low} = [0.005,2.000]$ Hz (b).

field) and $Re_c = \mathrm{O}(10^6)$. Therefore, the observed low-frequency peaks on the forces exerted over the wing are also connected to this spatial fluctuation of the wing-tip vortex behind the NACA0012 airfoil.

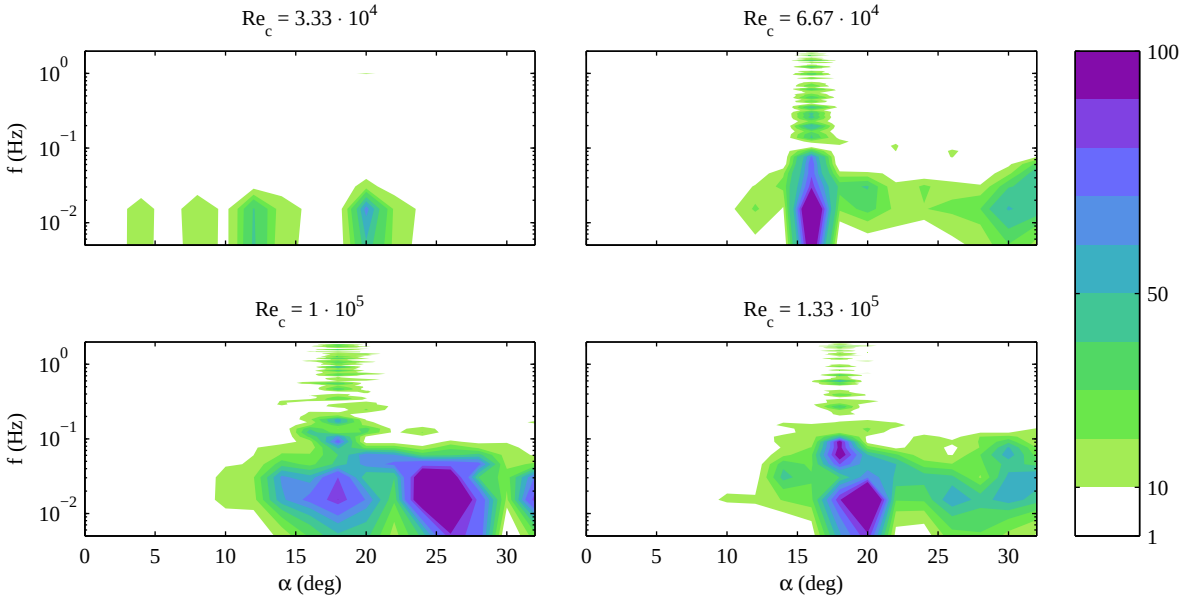

Figure 7: Normalized PSD for any value of Re_c at very low frequencies in the range between 0.005 and 2 Hz.

4.2. Dynamic response at high frequencies

Though the first two natural frequencies, f_{1st} and f_{2nd}, are significant and they dominate the whole dynamic response at $Re_c = 1 \cdot 10^5$ in our rigid model as shown in Fig. 4, several energetic and secondary frequencies are present for the two lowest Reynolds numbers near the first two natural frequencies but much less energetic than the natural ones. For this reason, we pay our attention on the interval of high frequencies, from 45 to 125 Hz. As we commented above for the low-frequency analysis, we filter again the PSD signal in the range of high frequencies for all the Reynolds numbers and AoA. The results are depicted in Fig. 8 together with those shedding-vortex results given by Huang (9) and Lee (10) from Fig.

4. It is observed a reasonable good agreement between our results and those frequencies reported by these authors. As Re_c increases, and consequently vortex shedding frequencies, these secondary components in the force signal around f_{1st} and f_{2nd} smoothly increase their influence. For the highest Reynolds number, the power peak at f_{2nd} disappears, and a new frequency becomes important at ∼116.25 Hz.

Furthermore, Kim citekim2009 detected Tollmien-Schlichting waves for $Re_c \leq 1 \cdot 10^5$ in the laminar-to-turbulent transition in the boundary layer with a main frequency of 32 Hz in the vicinity of the leading edge for a NACA 0012 airfoil and small AoA. Regarding our results, a power peak near to this frequency is also detected for the two lowest Re_c, primarily at small angles of attack (see Fig. 4). Moreover, and according to their results, the shear layer instability wave increased its frequency with the Reynolds number up to 53 Hz and 88 Hz over the trailing edge. In our case, these unstable waves in the laminar shear layer may also explain the secondary frequencies observed beyond the natural ones in Fig. 8.

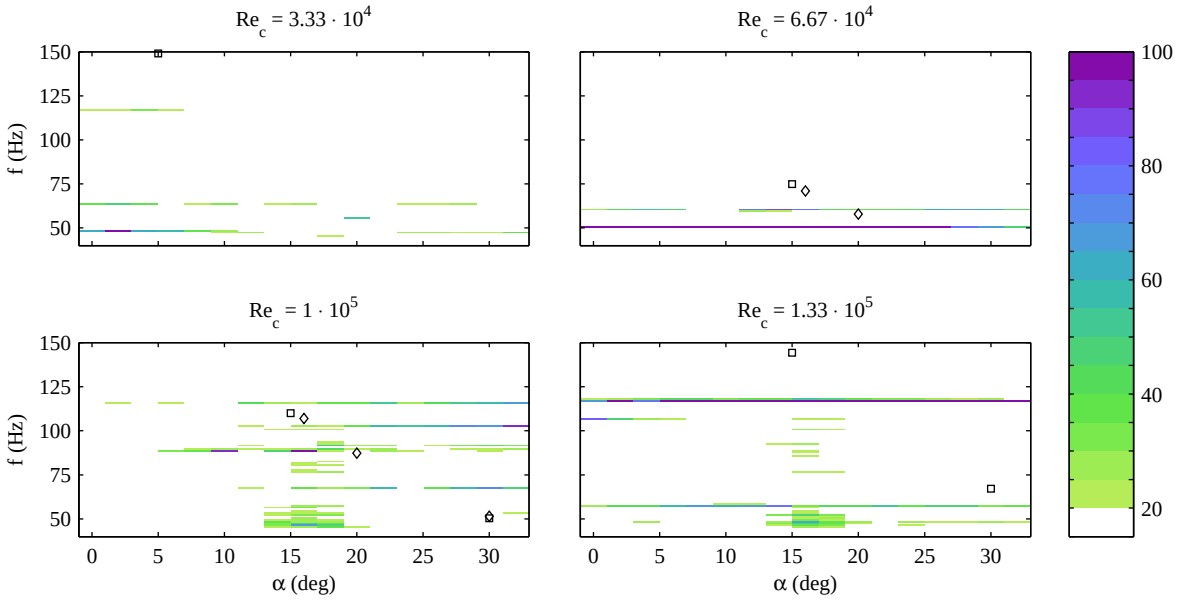

Figure 8: Normalized PSD for any value of Re_c at high frequencies in the range between 45 and 125 Hz.

5. Conclusions

The precise dynamic response of low-aspect-ratio NACA0012 airfoil at low Reynolds numbers has been characterized by a digital force sensor. We compute C_D, C_L and the PSD signal using the temporal evolution of the force measurements.

Regarding the PSD analysis, two natural frequencies f_{1st} and f_{2nd} of 28.25 Hz and 43.50 Hz, respectively, are found regardless the values of the AoA and Re_c and they correspond to the natural frequencies of the wing-base system model. This result seems to be evident since our model is rigid. It is also observed that the mean PSD level experiences a sudden increase with Re_c for the AoA slightly greater than the stall angle ($12° \leq \alpha \leq 22°$), particularly for Reynolds numbers greater than $1 \cdot 10^5$.

In addition, spectral density local peaks are found for frequencies lower than 0.2 Hz for any value of Re_c. These low-level frequencies appear approaching stall and they can be observed in the wing-tip phenomenon that produces a random movement of the vortex core behind the wing. Finally, high frequencies close to $O(10^2)$ Hz are linked to the formation and emission of coherent (unstable) turbulent structures in the near field of the wake since they are in agreement with other authors' results.

6. Acknowledgements

This research has been supported by Proyecto Junta de Excelencia de la Junta de Andalucía, Grant number P11-TEP-7776. Authors thank Lucía Luque for her corrections in the English style.

References

[1] Abbott IH, von Doenhoff AE. Theory of wing sections. Dover Publications, Inc., New York; 1959.

[2] Mueller TJ. Aerodynamics measurement at low Reynolds numbers for fixed wing micro-air vehicles. Hessert Centre for Aerospacial Research, Department of Aerospace and Mechanical Engineering, University of Notre Dame, Indiana (USA); 1999. .

[3] Mueller TJ, Torres GE. Aerodynamics of low aspect ratio wings at low Reynolds numbers with application to micro-air vehicles design an optimization. Hessert Centre for Aerospacial Research, Department of Aerospace and Mechanical Engineering, University of Notre Dame, Indiana (USA); 2001. .

[4] Lee T, Su YY. Wing tip vortex control via the use of a reverse half-delta wing. Experiments in Fluids. 2012;52:1593–1609.

[5] Lee T, Pereira J. Modification of static-wing tip vortex via a slender half-delta wing. Journal of Fluids and Structures. 2013;43:1–14.

[6] Gad-el Hak M. Control of low-speed airfoil aerodynamics. AIAA Journal. 1990;28(9):1537–1552.

[7] Mueller TJ. Low Reynolds number vehicles. AGARD-AG-288; 1985. .

[8] Huang RF, Lee HW. Effects of freestream turbulence on wing-surface flow and aerodynamic performance. Journal of Aircraft. 1999;36(9):965–972.

[9] Huang RF, Lin C. Vortex shedding and shear-layer instability of wing at low-Reynolds numbers. AIAA Journal. 1995;33(8):1398–1403.

[10] Lee HW, Huang RF. Frequency selection of wake flow behing a NACA 0012 wing. Journal of Marine Science and Technology. 1998;6(1):29–37.

[11] Huang RF, Lee HW. Turbulence effects on frequency characteristics of unsteady motions in wake of wing. AIAA Journal. 2000;38(1):85–93.

[12] Yen SC, Huang LC. Flow patterns and aerodynamics performance of unswept and swept-back wings. Journal of Fluids Engineering. 2009;131(11):111101–1–10.

[13] Yarusevych S, Sullivan PE, Kawalls JG. On vortex shedding from an airfoil in low-Reynolds-number flows. Journal of Fluid Mechanics. 2009;632:245–271.

[14] Gerakopulos RJ. Investigating flow over an airfoil al low Reynolds numbers using novel time-resolved surface pressure measurements. Doctoral Tesis, University of Waterloo, Ontario (Canada); 2011. .

[15] Boutilier MSH, Yarusevych S. Parametric study of separation and transition characteristics over an airfoil at low Reynolds numbers. Experiments in Fluids. 2013;52(6).

[16] Mahbub Alam M, Zhou Y, Yang HX, Guo H, Mi J. The ultra-low Reynolds number airfoil wake. Experiments in Fluids. 2010;48:81–103.

[17] Zhou Y, Mahbub Alam M, Yang HX, Guo H, Wood DH. Fluid forces on a very low Reynolds number airfoil and their prediction. International Journal of Heat and Fluid Flow. 2011;32:329–339.

[18] Poirel D, Harris Y, Benaissa A. Self-sustained aeroelastic oscillations of a NACA 0012 airfoil at low-to-moderate Reynolds numbers. Journal of Fluids and Structures. 2008;24:700–719.

[19] Kim DH, Chang JW. Low-Reynolds-number effect on the aerodynamic characteristics of a pitching NACA 0012 airfoil. Aerospace Science and Technology. 2014;32(1):162–168.

[20] Poirel D, Yuan W. Aerodynamics of laminar separation flutter at a transitional Reynolds number. Journal of Fluids and Structures. 2010;26:1174–1194.

[21] Rojratsirikul P, Wang Z, Gursul I. Effect of pre-strain and excess length on unsteady fluid structure interactions of membrane airfoils. Journal of Fluids and Structures. 2010;26:359–376.

[22] Rojratsirikul P, Genc MS, Wang Z, Gursul I. Flow-induced vibrations of low aspect ratio rectangular membrane wings. Journal of Fluids and Structures. 2011;27:1296–1309.

[23] Moreau DJ, Brooks LA, Doolan CJ. The effect of boundary layer type on trailing edge noise from sharp-edged at plates at low-to-moderate Reynolds number. Journal of Sound and Vibration. 2012;331:3976–3988.

[24] PeiChong T, Joseph PF. An experimental study of airfoil instability tonal noise with trailing edge serrations. Journal of Sound and Vibration. 2013;332:6335–6358.

[25] Moreau DJ, Prime Z, Porteous R, Doolan CJ, Valeau V. Flow-induced noise of a wall-mounted finit eairfoil at low-to-moderate Reynolds number. Journal of Sound and Vibration. 2014;333:6924–6941.

[26] Devenport WJ, Staubs JK, Glegg SAL. Sound radiation from real airfoils in turbulence. Journal of Sound and Vibration. 2010;329:3470–3483.

[27] Ikeda T, Atobe T, Takagi S. Direct simulations of trailing-edge noise generation from two-dimensional airfoils at low Reynolds numbers. Journal of Sound and Vibration. 2012;331:556–574.

[28] Bertagnolio F, Fischer A, Zhu W. Tuning of turbulent boundary layer anisotropy for improved surface pressure and trailing-edge noise modeling. Journal of Sound and Vibration. 2014;333:991–1010.

[29] Fedoul F, Parras L, del Pino C, Fernandez-Feria R. Experimental study of the aerodynamic characteristics of a low-aspect-ratio flat plate array in a configuration of interest for a tidal energy converter. Journal of Fluids and Structures. 2014;48:487–496.

[30] Martinez-Aranda S, Garcia-Gonzalez A, Parras L, Velazquez-Navarro J, del Pino C. Comparison of the Aerodynamic Characteristics of the NACA0012 Airfoil at Low-to-Moderate Reynolds Numbers for any Aspect Ratio. International Journal of Aerospace Sciences. 2016;4(1).

[31] Kline SJ, McClintock FA. Describing uncertainties in single-sample experiments. Mechanical Engineering. 1953;75(1):3–8.

[32] Goldstein RJ. Fluid Mechanics Measurements. Hemisphere Publishing Corporation, USA; 1983.

[33] Ngo HT, Barlow LE. Lifting surface with active variable tip member and method for influencing lifting surface behavior therewith. United State Patent No. US 6.394.397 B1; 2002. .

[34] Dalley JW, Ripperger EA. Experimental values of natural frequencies for skew and rectangular cantilever plates. Def. Res. Lab. Rept. DRL-231, CF-1359, University of Texas (USA); 1954. .

[35] Warburton GB. The vibration of rectangular plates. Proc Inst Mech Eng. 1954;168(12):371–384.

[36] Yarusevych S, Boutilier MSH. Vortex shedding of an airfoil at low Reynolds-numbers. AIAA Journal. 2011;49(10):2221–2227.

[37] Kim DH, Yang JH, Chang JW, Chung J. Boundary Layer and Near-wake Measurements of NACA 0012 Airfoil at Low Reynolds numbers. In: 47th AIAA Aerospace Sciences Meeting; 2009. .

[38] del Pino C, Lopez-Alonso JM, Parras L, Fernández-Feria R. Dynamics of the wing-tip cortex in the near field of a NACA 0012 airfoil. The Aeronautical Journal. 2011a;115(1166).

[39] Roy C, Leweke T. Experiments on vortex meandering. Technical Report 111-4 STREP, Fundamental Research on Aircraf Wake Phenomena CNRS-IRPHE. 2008;.